

PREDICTION OF PETROPHYSICAL PARAMETERS IN SANDSTONES BY USE OF SEM/IMAGE ANALYSIS

Reidar Bøe, Svein Mjaaland, Erik Lieng, Torleif Holt, Dag Wessel-Berg.
SINTEF Petroleum Research, N-7465 Trondheim, Norway.

Abstract

Attempts are made to conduct a multidisciplinary approach to provide petrophysical data from thin sections of reservoir sandstones by combined scanning electron microscopy (SEM) and advanced digital image analysis. Pore geometry data are obtained from mosaics of 16 backscattered electron (BSE) images, and both bulk- and pore surface mineralogy are determined by combining BSE and X-ray element distribution images.

Pore geometrical parameters produced from thin sections by this technique are compared with experimental data measured on corresponding core plugs. The data used in this study are mainly from Jurassic sandstones from the Frøy and Rind Fields in the Southern Viking Graben, but porosity data from Jurassic reservoir sandstones, Mid-Norwegian Continental Shelf, has also been included.

The analyses show that image porosity is consistently lower than He-porosity derived from plugs, but it can be calibrated to He-porosity by adding 55 per cent of the clay content, and thus account for micropores beyond the resolution in the SEM images.

Several pore geometrical parameters exhibit a strong correlation with permeability and can be used for prediction. These include macro porosity, specific pore surface area and the median pore area determined from a cumulative pore size distribution curve. Multiple linear regression analysis including these parameters produced an even stronger relationship with permeability. Data obtained from a modified version of the Kozeny – Carman equation also show a strong correlation to plug measurements.

By using a simple capillary tube model and estimating the pore throat radius for each macropore recorded by image analysis, capillary pressure curves were produced. They largely preserve the same sequence as those obtained from plug measurements. The relative position is mainly controlled by the irreducible wetting phase saturation, defined as the ratio between estimated microporosity and total porosity. Correlation with end point saturation (12 bars) revealed that in this connection only 40 per cent of the quantified clay should be considered as microporosity.

Wettability tests involving oils with different additives revealed that the wettability could be modified from strongly water wet to neutral and oil wet depending on the type of additive and of the surface mineralogy of the sandstone plugs. The results obtained indicate a potential for development of a method for wettability predictions based on knowledge of surface mineralogy and fluid properties.

Introduction

Efforts are made to conduct a multidisciplinary approach to provide petrophysical data from thin sections of reservoir sandstones. This involves close co-operation by geologists, chemists, mathematicians and physicists. This study focuses on providing estimates of parameters like porosity, absolute permeability, irreducible wetting phase saturation, capillary pressure curves, wettability and fluid distribution in sandstones pore network, and to use image analysis data to interpret anomalous log responses.

Numerous thin sections are routinely produced from cored intervals in reservoir zones, sometimes with only 25 cm interval. SEM-image acquisition and generation of pore geometrical parameters are fast and relatively cheap, and may become an important method to rapidly provide petrophysical data as a supplement to traditional plug measurements. Quantification of pore surface mineralogy is more time consuming, but it is likely that some reservoir quality parameters depending on mineralogy better can be explained by pore surface mineralogy data than mineralogy determined by common techniques (e.g. XRD and modal analysis).

Methodology

The technique used for quantification of pore geometry data and bulk- and pore surface mineralogy is based on a combination of scanning electron microscopy and image analysis. The analyses are performed on carbon-coated, polished thin sections produced from epoxy impregnated end cuts of horizontal plugs using a JEOL 733 scanning electron microscope combined with a NORAN Voyager energy dispersive X-ray analyser (EDX). Image acquisition was conducted with an accelerating voltage of 15 kV, and both backscattered electron (BSE) images and X-ray images were acquired.

Quantitative image analysis was performed on the digital SEM-derived images by means of a Kontron KS400 image analyser. It was applied to produce pore geometrical parameters as well as bulk- and pore wall mineralogy. The BSE images have the format 512×512 pixels (picture elements) and the X-ray images 256×256 pixels.

Image analysis is routinely carried out on images acquired at a fixed magnification of X60. A single image of this magnification covers only 4 mm², less than a half per cent of the cross section of a 1.5" plug. On the scale of a thin section, a sandstone is not homogeneous, requiring that several images be analysed to obtain a statistically representative sample. The images may be distributed randomly or cover parts of the thin sections in a more systematic manner. At Sintef Petroleum Research we routinely make mosaics of 16 (4×4) images of X60 magnification. This is done automatically; the image analysis system controls the movement of the sample stage. This approach minimizes edge effects of the images on pore and grain parameters. The format of the mosaic image is 2048×2048 pixels, and it covers as much as 0.5 cm² of the thin section. This may not be sufficient to account for all heterogeneities, and larger mosaics consisting of 64 images can be produced for heterogeneous rock samples.

In the backscattered electron image some constituents can be identified from their grey level, which is controlled by their ability to absorb electrons (Dilks and Graham, 1985). However, minerals with similar properties cannot be distinguished exclusively by means of grey level segmentation. A further discrimination of minerals can be obtained by means of X-ray analysis (Minnis, 1984; Fens and Clelland, 1990). A software program combines the BSE-image with X-ray images that show the distribution of some common elements (Si, Al, Ca, Mg, Na, K, Fe, S, P, Zr, Ti and Ba), identifies all minerals automatically, and produces a colour-coded mineralogy image. Incorrectly identified minerals are corrected interactively and the rock mineralogy calculated. In order to enable identification of thin rims of pore-lining clay the magnification of images used for quantification of mineralogy had to be increased to X120 or larger, and the images are located in the centre of each of the 16 images composing the mosaic image.

Bulk mineralogy determined by image analysis corresponds to traditional petrographical analyses of sandstones, where mineralogy is quantified by weight per cent (XRD) or by area in 2D-sections (modal analysis). However, it is likely to believe that some reservoir quality factors depending on mineralogy best can be explained by the mineral proportions which are in direct contact with the pore fluid, i.e. the pore wall or pore surface mineralogy. By further processing of the bulk mineralogy image a pore wall mineralogy map can be produced and the pore wall mineralogy calculated (Boassen and Leith, 1993).

Samples analysed

The data used in this study are mainly from Jurassic sandstones (BRENT Group, Tarbert and Ness Fm) from the Frøy and Rind Fields in the Southern Viking Graben. Porosity data from Jurassic reservoirs sandstones (Tofte and Tilje Fm), Mid-Norwegian Continental Shelf, has also been included. Four samples of the last category were applied for a wettability study together with a standard Berea sandstone.

Pore geometry and porosity

According to the Delesse principle (Underwood, 1970) volume fractions can be obtained by measuring area fractions on 2-dimensional sections, and 3-dimensional, curved surfaces can be represented by the trace lines in a cross-cutting plane section. Porosity can therefore be determined by image analysis of a thin section as the ratio between pore area and total area.

Pores have generally a more complicated shape than detrital grains, and pore parameters, like for instance pore size, can be defined and measured in many different ways. We routinely measure pore size as

the area of continuous pore space as it is recorded in the 2D-image, and do not split branched pores by putting any restrictions of minimum width of the branches connecting different parts of a pore.

The smallest pores recorded in a BSE image (X60) obtain the size of one pixel (picture element), i.e. $11.51 \mu\text{m}^2$. Pores smaller than 10 pixels (i.e. $115.1 \mu\text{m}^2$) are defined as micropores, while pores consisting of 10 pixels or more represent the macro pores. The total number of pores recorded in a mosaic image is generally in the range 6,000 – 10,000.

Sandstone samples with similar porosity may possess completely different properties. For instance, sample A (see below) represents a fine-grained sandstone with He-porosity 19.8% and permeability 27.5 mD, and sample B is a medium grained sandstone with He-porosity 20.0% and permeability 1300 mD. Obviously, porosity alone does not control permeability. This can be due to differences in the architecture of the pore network, factors like pore size and pore throat distribution and pore connectivity. The last two cannot easily be obtained from thin sections, but pore-size distribution can be derived and presented in several ways:

- In a frequency diagram showing the number of pores recorded in pre-defined pore-size classes.
- In a histogram showing the amount of pore area distributed in the different pore-size classes.
- As a cumulative curve resembling that of a grain size distribution curve.

The pores are divided into 40 pore-size classes ranging from $115.10 \mu\text{m}^2$ to $10,000,000 \mu\text{m}^2$. The division is done automatically along a logarithmic scale, and the size of each class therefore increases with increasing pore size.

Examples of pore size distributions for sample A and B are given in Figure 1. The frequency distribution diagrams show the number of pores in each pore size class and are completely different from those that illustrate the distribution of pore area in the same classes. Evidently a large number of small pores contribute little to the total pore area, while a small number of large pores may account for most of the pore space. The corresponding cumulative pore size distribution curves are also given. Such a curve is generated by successively adding the percentage of pore area recorded in each pore, starting with the smallest pore sizes. Thus it shows the percentage of pore space smaller than a given pore size.

The median pore size A_{50} corresponds to the 50 per cent value on the cumulative curve, and pores smaller than A_{50} constitute 50 per cent of the macropore area. While pore size calculated as arithmetic mean is significantly influenced by the large number of small pores, the median pore size better accounts for the significant contribution from a small number of large pores and has a stronger influence on permeability.

It is experienced that image porosity is generally lower than helium porosity measured on corresponding plugs (Fig. 2). The reason is that abundant sub-resolution microporosity accompanies clay minerals (e.g. Nadeau and Hurst, 1991; Hurst and Nadeau, 1995). The image porosity has therefore to be calibrated to He-porosity by adding a certain percentage of the recorded clay content. It is then essential that the analysed images are representative for the corresponding plugs, and distinctly heterogeneous samples are excluded. At this scale sandstones are seldom quite homogeneous, and porosity estimated from images and He-porosity that give different results may both be correct for the sample volume or area that each represents. The calibration was therefore based on the minimum average deviation from the unit line ($y = x$) for 75 sandstones from 8 wells from the southern Viking Graben and the Mid-Norwegian Continental Shelf.

The result from this analysis was that a “calculated porosity” (or “total porosity”) which better approximates He-porosity is obtained by considering 55 per cent of the clay content as microporosity and adding this to the recorded image porosity. Similarly, “calculated microporosity” is derived by adding the same proportion of clay to the recorded microporosity. This “clay” is discriminated by thresholding grey levels between pore space and quartz in the mosaic images. As long as kaolinite represents the dominating clay cement this technique works well, but in some of the samples substantial amounts of Fe-chlorite (higher grey level than quartz) were present. It was therefore necessary to include chlorite obtained from quantitative microanalysis. In later work also chlorite has been discriminated and quantified from the mosaic images.

Samples from different fields or wells may show different distributions slightly deviating from the 55% rule. The reason is that different types and distributions of clay minerals may contain different amounts of microporosity beyond the resolution in the images. If sufficient plug measurements are available, a control or new calibration should be performed for each field, well or formation.

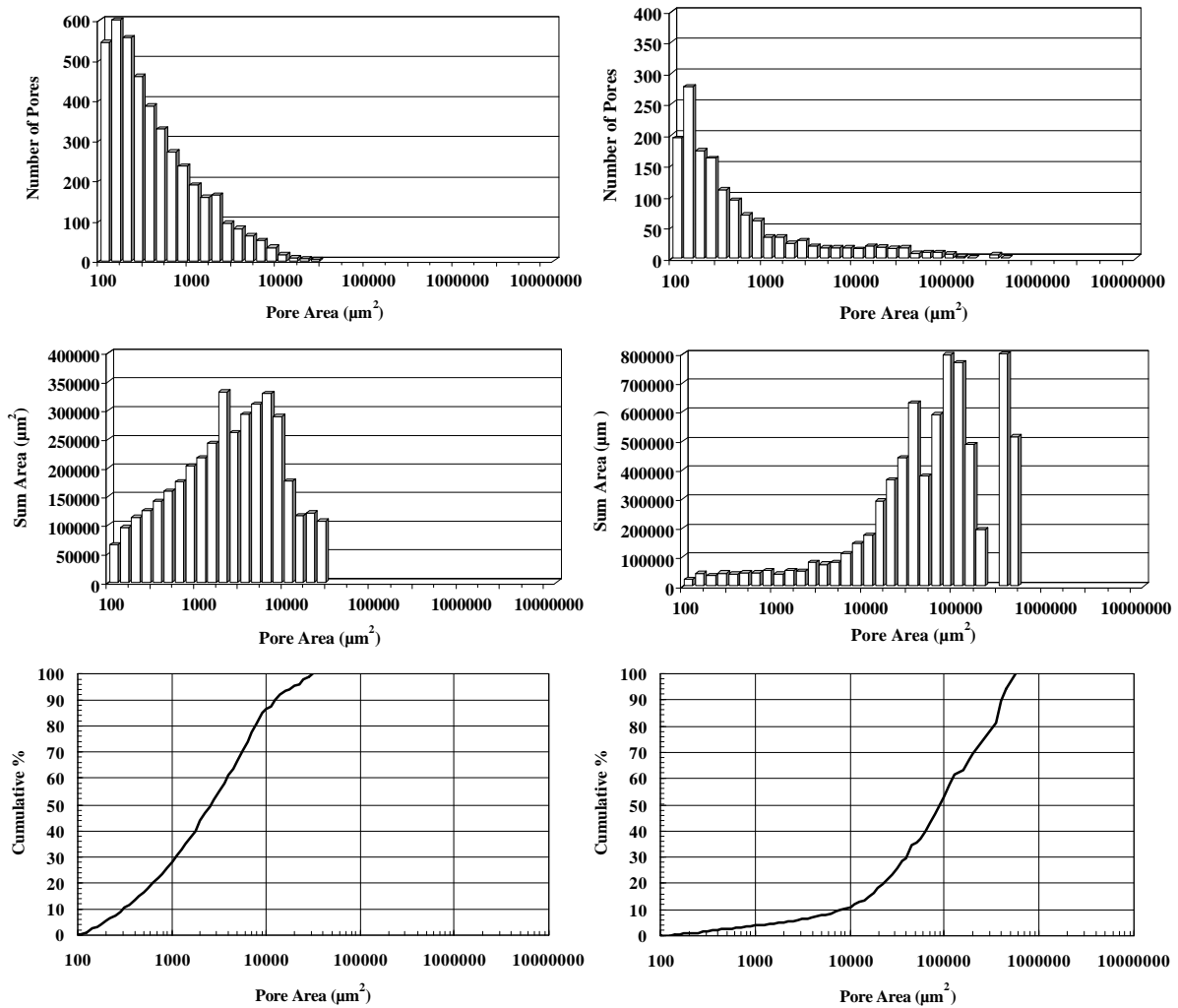


Figure 1. Pore size distribution diagrams for sample A (left) and B (right). The frequency distribution diagrams (up) show the number of pores in each pore size class, and the histograms (centre) show the distribution of pore area in the same classes. The large number of small pores contributes little to the total pore area. The lower diagrams are cumulative pore size distribution curves showing the percentage smaller than the corresponding pore size.

Permeability

Sandstones with similar porosity may have completely different transport properties. Still a good correlation between porosity and permeability is frequently observed, and porosity is commonly used for prediction of permeability. As shown above, image analysis makes it possible to quantify several kinds of porosity, and Figure 3 demonstrates their relationship to permeability (Klinkenberg corrected air permeability measured on horizontal plugs).

Micropores do not contribute to the effective part of the pore network that controls the transport properties. They are frequently related to clay cement precipitated in intergranular space, and have therefore a negative effect on permeability ($R^2 = 0.59$, Fig. 3D). A distinct positive relationship exists between permeability and both the estimated total porosity ($R^2 = 0.47$, Fig. 3A) and the image porosity ($R^2 = 0.77$, Fig. 3B), but since they include microporosity, the correlation is not as good as that shown by the macro porosity ($R^2 = 0.79$, Fig. 3C) which, to a larger extent, represents the effective porosity.

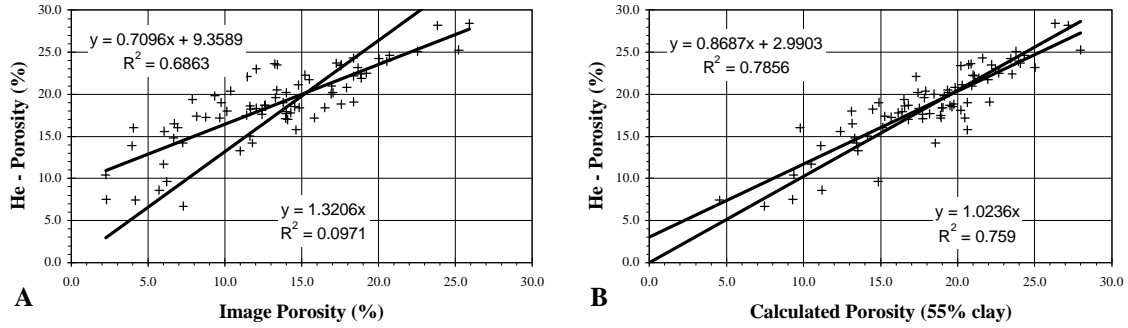


Figure 2. A) Scatter diagram illustrating that the image porosity is consistently lower than Helium porosity measured on plugs. B) If 55 per cent of the clay content is considered to represent microporosity and therefore added to the image porosity, a better correlation with He-porosity is obtained. Two regression lines with equation and correlation coefficients are included in each diagram. One of the lines represents forced fit through the origin.

If the ratio between the estimated micro- and total porosity is considered, this relationship is slightly improved ($R^2 = 0.81$, Fig. 4D). Also the mean equivalent circular diameter (the diameter of a circle with an area equivalent to the area of a pore) measured on individual pores larger than $115.10 \mu\text{m}^2$ (i.e. macro pores correlates well with permeability ($R^2 = 0.81$, Fig. 4B). The median pore size A_{50} is less affected by the large number of small pores and exhibits a stronger correlation with permeability ($R^2 = 0.89$, Fig. 4A). Even stronger is the correlation shown by the specific pore surface area (the ratio between the total pore perimeter and the sum of pore area of all pores larger than $115.10 \mu\text{m}^2$) ($R^2 = 0.90$, Fig. 4C).

Multiple linear regression analysis including macro porosity (Φ), median pore size (A_{50}) and specific pore surface (S_s) improves the permeability (k_{MLR}) estimate slightly:

$$k_{MLR} = 10^{(0.01733\Phi - 9.23772S_s + 0.61925 \log A_{50} + 0.71351)} \quad (1)$$

Figure 5A illustrates the relationship between permeability calculated from this equation and permeability measured on plugs ($R^2 = 0.9153$). The main contribution is from specific pore surface.

The Kozeny – Carman equation (Ruzyla 1986) represents an alternative method to obtain permeability (k_{CK}) from pore geometry data:

$$k_{CK} = \frac{A_f^3}{k'(1 - A_f)^2 \left[\frac{4}{p} \times \frac{P}{A_p} \right]^2} \times 1013 \quad (2)$$

A_f is fractional porosity, k' is the Kozeny constant, and $4/\pi$ is a statistical factor which is used when 3D information is obtained from 2D sections. P/A_p is the relationship between total pore perimeter and the total macropore area, i.e. the specific pore surface. Permeability is generally expressed in millidarcy (mD), and in order to get square micrometers converted to this unit it is, according to Ehrlich et al. (1991), necessary to use the factor 1013.

In the present study a modified version of the Kozeny – Carman equation has been used. For fractional porosity the macro (“effective”) porosity is applied. The expression $(1 - A_f)^2$ in the denominator is neglected, and the exponent 3 in the numerator is replaced by 2.1. For packed, unconsolidated sand a Kozeny constant of 5 is recommended (Dullien, 1979). From another data set from Jurassic sandstones (BRENT Group, Southern Viking Graben) this factor was calculated to 2.7 for consolidated sand.

Figure 5B illustrates the relationship between the permeability derived from the Kozeny – Carman equation and the permeability measured on plugs ($R^2 = 0.89$). The calculated values deviate somewhat from

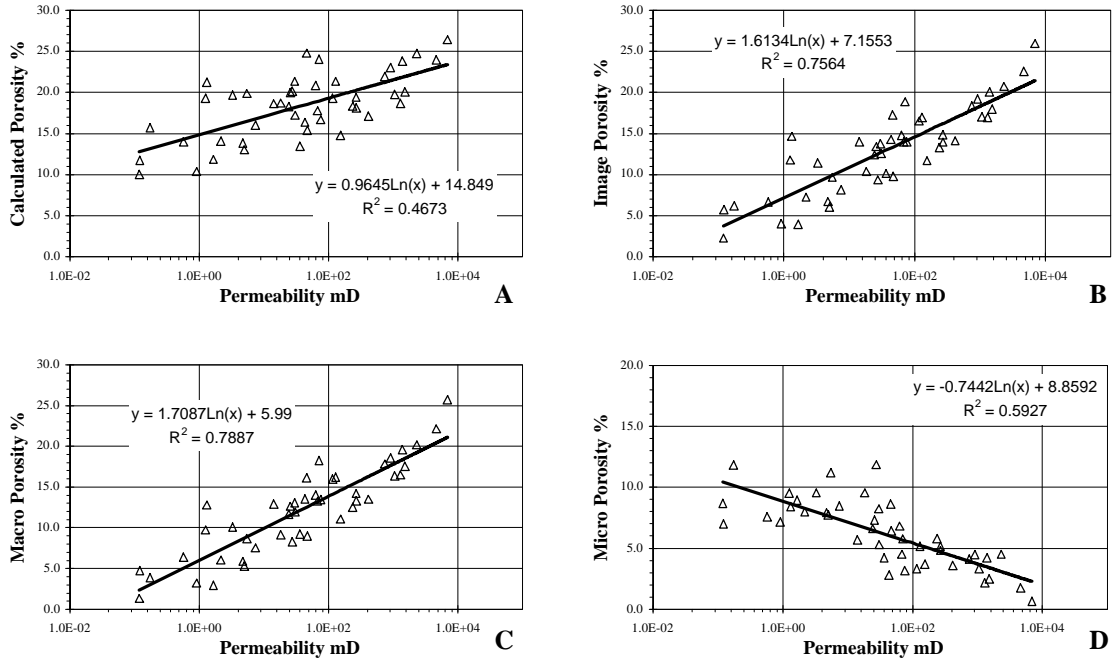


Figure 3. Scatter diagrams illustrating relationships between permeability (Klinkenberg corrected) and various types of porosity. Equation of regression lines (logarithmic) and correlation coefficients are included in each diagram. The samples are Jurassic sandstones from the Southern Viking Graben).

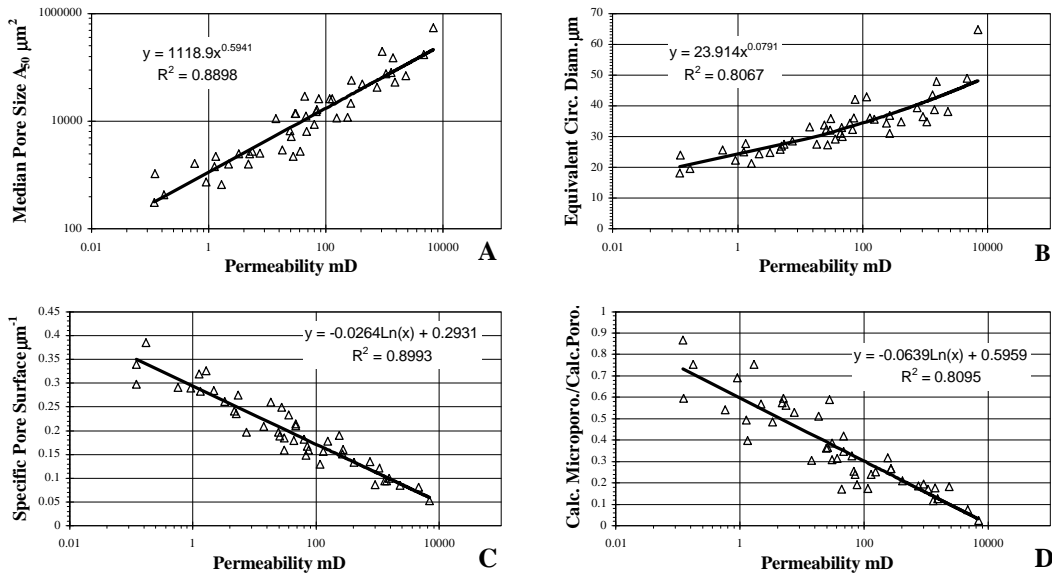


Figure 4. Scatter diagrams illustrating relationships between permeability (Klinkenberg corrected) and A) the median pore size, B) equivalent circular diameter, C) specific pore surface and D) the ratio between the estimated microporosity and estimated total porosity. Equation of regression lines (power functions in upper diagrams and logarithmic in lower diagrams) and correlation coefficients are included.

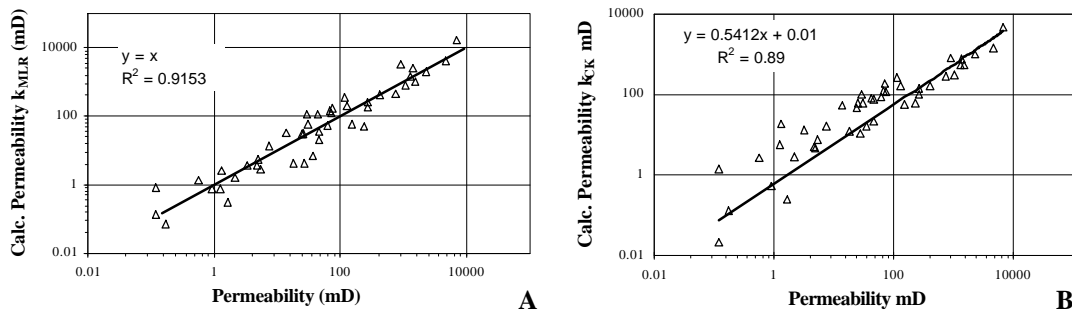


Figure 5. A) Scatter diagram (log-scale) illustrating the relationship between permeability calculated by multiple regression analysis (Eq. 1) and permeability measured on plugs (Klinkenberg corrected). The regression line in the diagram corresponds to the unit line. B) Forced fit linear correlation between permeability calculated by means of a modified version of the Kozeny – Carman equation and plug permeability.

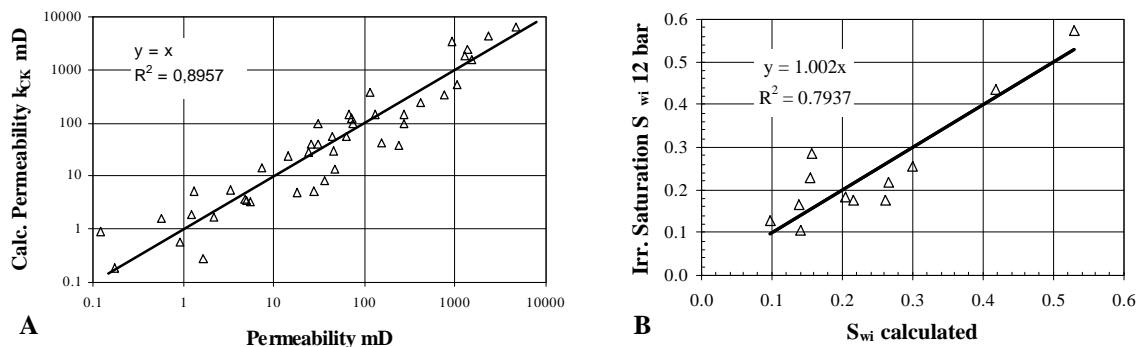


Figure 6. A) Scatter diagram showing the distribution of data points estimated from a modified version of the Kozeny – Carman equation (Eq. 2) with exponent 0.6 in the numerator, adjusted to the unit line. B) Scatter diagram illustrating the relationship between the calculated irreducible saturation and the corresponding saturation measured at 12 bars (porous plate technique). The correlation line (forced fit through origin) lies close to the unit line.

the unit line. However, by simple normalization of the data to this line, small adjustments of the equation can produce values that better correspond to the plug measurements. The best correlation is then obtained when 0.6 is applied as exponent in the numerator (Fig. 6A). The Kozeny - Carman equation is especially applicable in connection with image analysis if one wishes to determine palaeo-permeability, the permeability prevailing prior to the deposition of a cement, or to quantify the effect of cement on permeability. Permeability can be calculated from pore parameters measured both before and after removal of cement from the SEM-image (back-stripping).

Irreducible saturation

Attempting to predict drainage capillary pressure (P_c) curves from SEM images, the irreducible wetting phase saturation is crucial for their location in the P_c – saturation diagram. We have defined a calculated irreducible saturation S_{wi} as the ratio between the calculated microporosity (recorded microporosity plus the contribution from clay) and the calculated total porosity. The data set used for calibration is small. Only twelve samples from the Frøy and Rind Fields were available. The irreducible wetting phase saturation was determined on cleaned samples at 12 bars by the porous plate technique.

It would be most convenient if the contribution of microporosity from the clay corresponded to the percentage determined from the calibration of porosity with He-porosity, i.e. 55 per cent. However, when

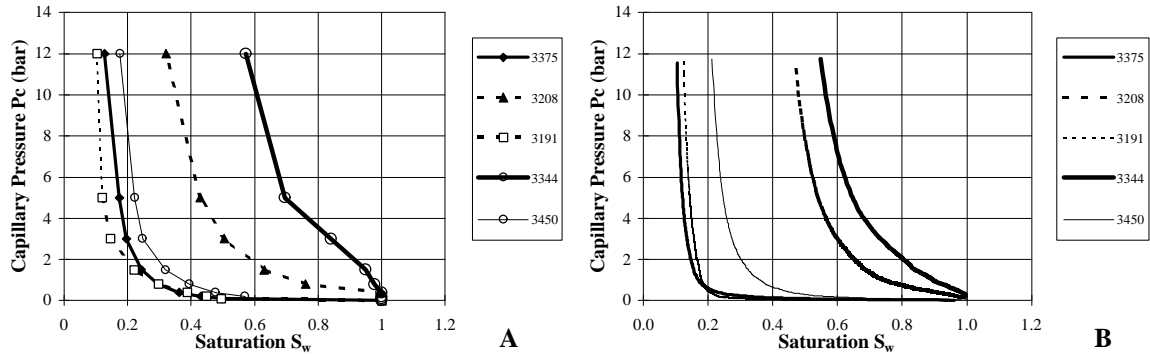


Figure 7. A) Drainage capillary pressure curves for five sandstone samples determined by the porous plate technique. B) Capillary pressure curves generated from pore geometry data obtained by combined SEM/image analysis of thin sections.

calibrating S_{wi} with irreducible saturation from the drainage experiments, 40 per cent microporosity contribution from clay gave the best fit (Fig. 6B) both with the unit line and the correlation line ($R^2 = 0.79$). The reason is probably that the largest micropores recorded in the images (1 – 9 pixels) as well as some of the microporosity accompanying clay do not contain capillary fluid at 12 bars.

Capillary pressure curves

The capillary pressure (P_c) in a two phase fluid system in a porous medium is per definition the difference between the fluid phase pressures at the prevailing conditions. P_c is a macroscopic, or Darcy scale, petrophysical parameter accounting for complicated properties of the micro-structure and the microscopic two-phase fluid distribution. However, at a given position in a porous medium, the (macroscopic) capillary pressure is usually given as a function of fluid saturation alone, and is referred to as “the capillary pressure curve”. In addition, one also distinguishes between primary, secondary, etc. capillary pressure curves in processes with non-monotonous saturation changes. All curves referred to below are primary curves.

In numerical simulations of two-phase flow in porous media the capillary pressure curves are part of the input parameters, and capillary forces will in general dominate the flow behaviour on small to moderate scales (e.g. plug to bed scale) at realistic reservoir flow rates. For field scale simulations of flow in hydrocarbon reservoirs one generally needs to apply numerical grid blocks much larger than plug and bed scale, and now gravitational and viscous forces dominate over the capillary forces. However, applied field scale petrophysical input parameters are average, or upscaled, values accounting for the variation of small scale petrophysical parameters in the large scale numerical grid block. In particular, the upscaled relative permeability is largely a result of the fine scale distribution of capillary pressure curves. Field scale relative permeabilities are important parameters in the prediction of hydrocarbon field behaviour, especially the (effective) relative permeability saturation endpoints. Therefore, the highest possible quality for these input data should be sought. This can be achieved by providing an extensive set of plug scale capillary pressure curves (serving as input parameters in the upscaling routine).

In this study plug scale porous plate measurements of drainage capillary pressure curves have been compared with capillary pressure curves generated from pore geometry data from thin-sections. The model applied here to represent the microscopic porous medium is the simplest possible; a bundle of capillary tubes. The distribution of tube cross-sectional areas is based on the distribution of pore areas obtained from the thin section measurements.

Since the capillary pressure is not predominantly influenced by the pore size or pore size distribution, but by the corresponding pore entry diameters or pore throats which are not possible to quantify directly from thin section, it is necessary to establish a procedure for estimation of pore throats. To start with, the radius of the equivalent circular diameter (r_e) is calculated for each pore after correcting the pore area for the cut effect (the thin section only occasionally reveals the largest cross section through a pore):

$$r_c = \sqrt{\frac{A}{0.67 \times p}} \quad (3)$$

A linear relationship between the size of pores and corresponding throats is unlikely. One may assume that the throats are one or two orders of magnitude smaller than the pores, but the relationship may be modified by other, quantifiable parameters. One hypothesis is that the crookedness or roughness of the pores may affect the sizes of the pore throats, making them relatively smaller with increasing crookedness. This can be quantified as the ratio between pore perimeter P and pore area A (i.e. the specific pore surface area), but as this also depends on size, the difference between this ratio and the corresponding ratio of the equivalent circle is applied: $(P/A_{\text{pore}} - P/A_{\text{circle}})$. The calibration factor α introduced to obtain a “pore throat radius” $r = \alpha \times r_c$ was set to $\alpha = (1500 \times (P/A_{\text{pore}} - P/A_{\text{circle}}))^{-1}$.

Let the interfacial tension σ be 20 mN/m (this is a typical value for oil/water interface). The drainage capillary pressure curve can then be calculated as follows: Increase P_c until $P_c = 2\sigma/r$, where r is the largest pore throat radius. Thus this tube is invaded by the non-wetting phase. Record the relative area of this tube (i.e. to total bundle area), and plot it against P_c . Increase P_c further until the next tube is invaded, record P_c against invaded area relative to total, and proceed in this manner.

Figure 7A shows five capillary pressure curves determined from plug measurements in the laboratory (porous plate method). Visual inspection of the cores indicated that the sandstones were relatively homogeneous. Thin sections were prepared from samples collected close to the plugs or from end cuts. In Figure 7B the corresponding capillary pressure curves generated from pore geometry data obtained from these thin sections are presented. It demonstrates that the curves have similar shapes, and the sequence of the curves is preserved apart from the two close samples with very low wetting phase saturations. Notice that the ranking sequence of the curves cannot be juggled by changing the calibration factor α .

The geometrical pore scale model is extremely simple, and obvious weaknesses can be documented. Possible effects of wettability are ignored, and pore connectivity is not taken into consideration. Furthermore, only drainage capillary pressure curves can be calculated. In a water injection hydrocarbon recovery process with water wetting reservoir rock, the (primary) imbibition capillary pressure curves should be applied. In spite of this, the results of the empirical comparison performed here are very promising. The SEM method is quick and relatively cheap compared with standard laboratory techniques.

Current research on this subject is concentrated in making an improved and more realistic model that also takes pore connectivity into account.

The use of pore surface mineralogy to quantify wettability

The fluid distribution inside a reservoir rock, oil, water system will depend on the properties of the rock surface and the composition of the fluids involved. Depending on the affinity of oil components to the mineral surfaces, oil components may adsorb and possibly make the surfaces more oil wet. The affinity between oil and mineral surfaces will be determined by the quantity and types of surface-active components in the oil, the brine composition and the properties of the surface minerals. The abundance and distribution of oil wet pore wall regions are assumed to determine the wettability, the flow characteristics and the residual oil in the porous medium.

The wettability of a rock/fluid system can possibly be predicted from the distribution of surface minerals, knowing individual mineral properties and the content of specific groups of components in the reservoir fluids. To develop a method to predict wettability along these principles is the goal of the present activity.

The effect of surface mineralogy and fluid composition is demonstrated by wettability tests using three different sandstones and three different fluid systems. Clay minerals dominated the surfaces of sandstones C and D, although the dominant types of clays were different (*cf.* Table 1). Quartz was the most abundant surface mineral of Berea. The fluid systems used were a NaCl brine and n-decane, either pure or with added oil soluble base or acid (Tweheyo et al., 1998).

The results from the Amott wettability tests are depicted in Figure 8. The reservoir cores C and D, both rich in surface clays exhibited a similar wettability for each fluid system. For oil without additives they were water wet, weakly oil wet with the organic base added to the oil and close to neutral with acid. The

Table 1. Pore surface mineralogy (percentage) for sandstone C and D and Berea sandstone determined by image analysis of thin sections.

Mineral	Sandstone C	Sandstone D	Berea
Quartz	42	20	62
Feldspars	3	18	5
Kaolinite	47	2	24
Fe-chlorite	0	43	0
Other clays	7	13	8
Other minerals	1	4	1

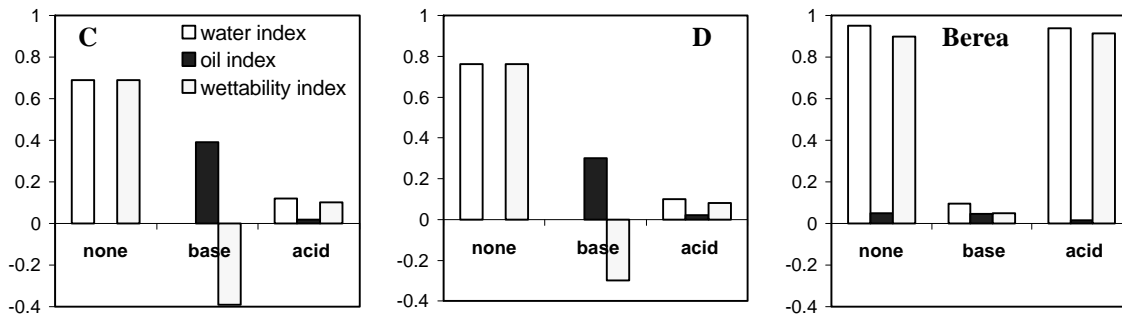


Figure 8. Amott wettability indexes for sandstones C and D and Berea sandstone, measured for different oil/brine systems.

Berea core remained water wet with added oil soluble acid, but shifted to neutral wettability with base. Core flooding experiments performed with the different rocks and fluid systems resulted in characteristic oil recovery profiles corresponding to the wettability of the systems (Tweheyo et al., 1998; Bøe et al., 1997).

With base added to the oil it is likely that the base swiftly diffused through the brine, and the positively charged part of the dissociated base adsorbed strongly on the rock surface, making the surface oil wet. Lower adsorption of the negatively charged acid molecules modified the wettability towards neutral. Less adsorption on quartz compared to clays could only modify the wettability on Berea to neutral when base was added to the oil. Dissociated acid molecules did not adsorb enough to modify wettability of Berea sandstone at all. The observed wettability transitions resemble wettability changes seen by Alveskog et al. (1998) by addition of a water-soluble anionic surfactant (n-dodecyl-o-xylene sulphonate) to the aqueous phase. In that work an abrupt change in wettability from water wet was observed close the critical micelle concentration. For oil soluble surface-active components the molecules have to diffuse through the aqueous phase in order to adsorb to the rock surface, and eventually modify the wetting conditions depending on the type of molecules and degree of adsorption. According to Kaminsky and Radke (1998) the equilibrium times involved in such mass transfer processes are short (hours) compared to the experimental times involved.

The results obtained indicate a potential for development of a method for wettability predictions based on quantitative mineralogy data from thin sections and knowledge about the surface-active components in the oil. Image analysis enables quantification of pore surface mineralogy in each pore. Information of surface properties of pore wall minerals, their abundance and distribution, as well as knowledge of fluid properties, can make it possible to establish a connection between pore surface mineralogy and sites with affinity to oil. Ongoing research has resulted in software that enables combination of pore surface mineralogy with mineral properties to produce surface charge maps. For a given pH in the brine the surface charge maps will automatically update. Attempts are made to use such maps for predictions of the distribution of pore fluids in the pore space. Such method for wettability prediction based on thin section data may become a useful tool for controlling wetting determined on core samples by conventional methods, and may also be used to predict wettability in reservoir intervals where conventional tests have not been made.

The effect of grain-coating chlorite on petrophysical log responses

In deeply buried sandstones chlorite coatings on the grains are reported to inhibit the diagenesis process and preserve porosity, thus maintaining good reservoir quality (Ehrenberg, 1993). Prediction of water saturation from resistivity logs may be complex in shaly sands. This is especially true in zones dominated by chlorite rims (Seyler, 1997). It is the chlorite distribution rather than the volume fraction that influences the resistivity log. Continuous pore lining, brine filled chlorite will give unrestricted path to the electrical current in an hydrocarbon zone, and thus a low resistivity on the log.

Attempts are made to improve the interpretation of resistivity logs in chlorite zones through detailed characterisation of mineral volumes and mineral distributions from analysis of thin sections.

Summary and conclusions

Attempts are made to provide petrophysical data from thin sections of reservoir sandstones by combined scanning electron microscopy and image analysis. Pore geometry data are obtained from mosaics of 16 backscattered electron (BSE) images, and both bulk- and pore surface mineralogy are determined by combining BSE and X-ray element images.

Numerous thin sections are routinely produced from cored intervals in reservoir zones. SEM-image acquisition and generation of pore geometrical parameters are fast and relatively cheap, and this method may become an important way to rapidly provide petrophysical data as a supplement to traditional plug measurements. Mineralogy determination is more time consuming than techniques like modal analysis (point counting of thin sections) and semi-quantitative X-ray diffraction analysis. However, it is likely that some reservoir quality parameters depending on mineralogy best can be explained by quantitative pore surface mineralogy data produced by combined SEM/image analysis of thin sections.

Image porosity is consistently lower than He-porosity derived from plugs, but micropores beyond the resolution in the SEM image can be accounted for by adding 55 per cent of the clay content. Permeability can be estimated using correlation lines determined by direct correlation with specific pore surface area ($R^2 = 0.90$) or the median pore area determined from a cumulative pore size distribution curve ($R^2 = 0.89$), by a relationship established by multiple linear regression analysis including macro porosity, specific pore surface, and median pore area ($R^2 = 0.92$), or by using a modified version of the Kozeny – Carman equation ($R^2 = 0.90$).

The irreducible wetting phase saturation is defined as the ratio between estimated microporosity and total porosity. Correlation with irreducible water saturation (12 bars) measured on plugs revealed that in this connection only 40 per cent of the quantified clay should be considered as microporosity. This indicates that the microporosity recorded in the SEM images plus some of the microporosity accompanying clay is not filled by the wetting phase at that high pressure.

By using a simple capillary tube model and estimating the pore throat radius for each macropore recorded by image analysis, capillary pressure curves that largely preserve the relative position of the curves were produced. Efforts are now being made to generate a new and more realistic model that takes care of the connectivity in the pore network.

Wettability tests involving oils with different additives revealed that the wettability could be modified from strongly water wet to neutral and oil wet depending on the type of additive and of the surface mineralogy of the sandstone plugs. The results obtained indicate a potential for development of a method for wettability predictions based on knowledge of surface mineralogy and fluid properties.

Acknowledgements

The authors would like to thank Elf Petroleum Norge for permission to use data and results from a research project conducted for them on samples from Frøy and Rind, and the Norwegian Research Council for financial support for further research through a strategic institute program on formation evaluation. We further acknowledge Statoil and Saga Petroleum asa for permission to use data from the Mid-Norwegian Continental Shelf, and Saga Petroleum asa for providing samples for the wettability study.

References

- Alveskog, P. L., Holt, T., and Torsæter, O. 1998: The effect of surfactant concentration on the Amott wettability index and residual oil saturation, *Journ. Petr. Sci. and Eng.*, p. 673.
- Boassen, T. and Leith, D.A. 1993: Reservoir modelling by the characterization of pore wall mineralogy. Abstract. 5th EAPG Conference. Stavanger.
- Bøe, R., Holt, T. and Torsæter, O. 1997: An experimental study of the relationship between rock surface properties, wettability and oil production characteristics, Paper SCA9739, Proc. 1997 Int. Symp. of the Society of Core Analysts, Calgary. Alberta, Sept. 7 - 10.
- Dilks, A. and Graham, S.C. 1985: Quantitative mineralogical characterization of sandstones by back-scattered electron image analysis. *Journ. Sed. Petrol.*, Vol. 55, No. 3, p. 347 - 355.
- Dullien, F.A.L. 1979: Porous media – fluid transport and pore structure. Academic Press, New York, pp. 396.
- Ehrenberg, S.N. 1993: Preservation of anomalously high porosity in deeply buried sandstones by grain-coating chlorite: examples from the Norwegian continental shelf. *AAPG Bulletin* 77, p. 1260 - 1286.
- Ehrlich, R., Etris, E.L., Brumfield, D., Yan, L.P. and Crabtree, S.J. 1991: Petrography and reservoir physics III: Physical models for permeability and formation factor. *Am. Ass. Petr. Geol. Bull.*, Vol. 75, No. 10, p. 1579 – 1592.
- Fens, T.W. and Clelland, W.D. 1990: Automated rock characterization using scanning electron microscopy/image analysis techniques. Europec 90, Haag 22 24 Oct. SPE 20920, p. 369 - 377.
- Hurst, A. and Nadeau, P. H. 1995: Clay microporosity in reservoir sandstones: an application of quantitative electron microscopy in petrophysical evaluation. *AAPG Bulletin*, Vol. 79, No. 4, p. 563 - 573.
- Minnis, M.M. 1984: An automatic point-counting method for mineralogical assessment. *Am. Ass. Petrol. Geol. Bull.*, Vol. 68, No. 6, p. 744 - 752.
- Nadeau, P. H. and Hurst, A. 1991: Application of back-scattered electron microscopy to the quantification of clay mineral microporosity in sandstones. *J. Sed. Petrol.*, Vol. 61, No. 6, p. 921 - 925.
- Kaminsky, R. and Radke, C.J. 1998: Water films, asphaltenes, and wettability alteration, Paper SPE 39087 presented at the SPE/DOE Symp. on IOR, Tulsa Ok., 19 - 22 April.
- Ruzyla, K. 1986: Characterization of pore space by quantitative image analysis. *SPE Formation Evaluation*, p. 389 - 398.
- Seyler, B. 1997: Low resistivity in Aux Vases sandstone reservoirs in the Illinois Basin linked to clay minerals coating sand grains, *Ann. AAPG-SEPM-EMD-DPA-DEG Conv. Dallas, Sept. 4 – 6. Pap. Abstr. A105 - A106.*
- Tweheyo, M.T., Holt, T. and Torsæter, O. 1998: An Experimental Study of the Relationship between Wettability and Oil Production Characteristics, *Proc. 5th Int. Symp. on Evaluation of Reservoir Wettability and its Effect on Oil Recovery*, Trondheim, June 22 - 24.
- Underwood, E.E. 1970: *Quantitative Stereology*. Addison – Wesley Publishing Company Inc., Reading, Massachusetts, pp. 274.